

Constraints on the detection of topological charge of optical vortices using self-reference interferometry

Siyao Wu, Ling Chen,^{*} Ruiping Jing, and Baocheng Zhang[†]

*School of Mathematics and Physics,
China University of Geosciences, Wuhan 430074, China*

Abstract

Self-reference interferometry of optical vortices using a Michelson interferometer is investigated in this paper. It is found that the detection of topological charge (TC) for the optical vortices is constrained by some physical conditions. We present these conditions through the theoretical analyses, numerical simulation and experimental results. For different parameters, the maximal detectable TCs are different, which is helpful for the measurement of TC in the practical application. Within the range allowed by the constrained conditions, we also study the detection of TC using the interference pattern of two-way optical vortex by changing the inclined angle of one mirror of the Michelson interferometer.

^{*}Electronic address: lingchen@cug.edu.cn

[†]Electronic address: zhangbaocheng@cug.edu.cn

I. INTRODUCTION

Since optical vortices were found [1, 2], their structure and property such as cylindrical symmetry, dark core at the center and so on in the propagation [3, 4] has been studied over the past few decades. The wave vector of the optical vortex rotates around the vortex center, which leads to an orbital angular momentum (OAM) appearing in the phase as $\exp(im\theta)$, where m is topological charge (TC) [5] and determines the OAM value ($m\hbar$) of the photon. The most familiar types of optical vortices are Laguerre-Gaussian (LG) beams, Bessel and Bessel-Gaussian beams, ring Gaussian beams and hypergeometric Gaussian beams, etc. They can be generated artificially by different methods, such as the geometrical optics model transformation method [6], the spiral phase plate method [7], the computer generated holographic method (CGH) [8], the spatial liquid-crystal modulation method (SLM) [9], and the metamaterial vortex producing method [10, 11] etc.

Optical vortices have been applied to many different situations, such as optical trapping [12, 13], optical communication [14, 15], microscopy imaging [16, 17], laser micromachines [18, 19], rotating velocity detection [20, 21], optical analogue for black hole [22, 23], and so on. In all these applications, TC or OAM of the optical vortex plays a key role, so it is very important to find out the value of TC.

In terms of measuring the TC, various techniques have been proposed, such as the diffraction grating method [24, 25], Doppler analysis [26], the metamaterial surface method [27, 28], interferometry [29–31] and so on. Different methods have their advantages and disadvantages. For example, in the interferometric method, the TC can be specified by the interference of a reference beam (such as a plane or spherical beam) and a detected vortex beam, as usually carried out in Mach-Zehnder interferometers [32–35]. Since the same frequencies in the interferometry are required for the two beams, the self-reference interferometry is advantageous to realize this point. Based on the interference resulting from splitting incident wave by Wollaston prism or birefringent plate, the optical vortex sign was determined by self-interference methods [36]. Recently, B. Lan et al. carried out the dislocation self-reference interferometry based on Michelson interferometer to measure the TC of the vortex beam [37]. In their method, the TC can be measured accurately and the additional reference beam is not required. However, they didn't realize the measurement limits of this technique, which provides the motivation for our work in this paper. We will show that

the measurable maximal value of TC using self-reference interferometry is affected by some physical parameters such as the radius of the beam and so on.

In this paper, we investigate the self-reference interferometry [37] through the theoretical and experimental avenues using a Michelson interferometer and discuss the measurement limits of this method. It is noted that the interference stripes will become fat when centers of the two vortex beams approach to each other, which limits the measurable values of the TC and has not been observed before. For presenting this, the paper is organized as followed. In the second section, we study the constraint on the detection for the TC of the optical vortex by theoretical analyses, numerical simulation and experimental demonstration. A fundamental constrained relation is given through purely theoretical analysis. At the same time, the constraint from the experimental conditions is analyzed. Within the allowed range by the constrained conditions, we discuss three different cases for the self-reference interference, and compare the simulated and experimental results in the third section. Meanwhile, we also discuss the capacity using the self-reference interferometry to detect whether two beams are parallel (whether the mirrors in the Michelson interferometer are vertical). Finally, we give the conclusion in the fourth section.

II. CONSTRAINT ON SELF-REFERENCE INTERFEROMETRY

We start with two vortex beams, one of which goes along the optic axis and another one goes with an inclined angle α (for its practical meaning, see the experimental setup in Fig. 1 which will be discussed later) from the optic axis. They can be described with the complex optical fields E_{OAM1} and E_{OAM2} as

$$E_{OAM1} = A_1 \exp(im_1\theta), \quad (1)$$

$$E_{OAM2} = A_2 \exp(im_2\theta' + ikrsin\alpha), \quad (2)$$

where A_1 , A_2 and m_1 , m_2 denote the amplitude and TCs of the two vortex beams, respectively. θ and θ' are the azimuthal angles of the vortex beams, k is the wave vector, and r is the radial distance on the transverse plane perpendicular to the propagation axis. The additional phase $ikrsin\alpha$ originates from the inclination of one beams from another one during the propagation and the value is obtained by projecting the inclined wave vector on the transverse plane. This term $ikrsin\alpha$ is equivalent to that term called as φ_{carry} in Ref. [37],

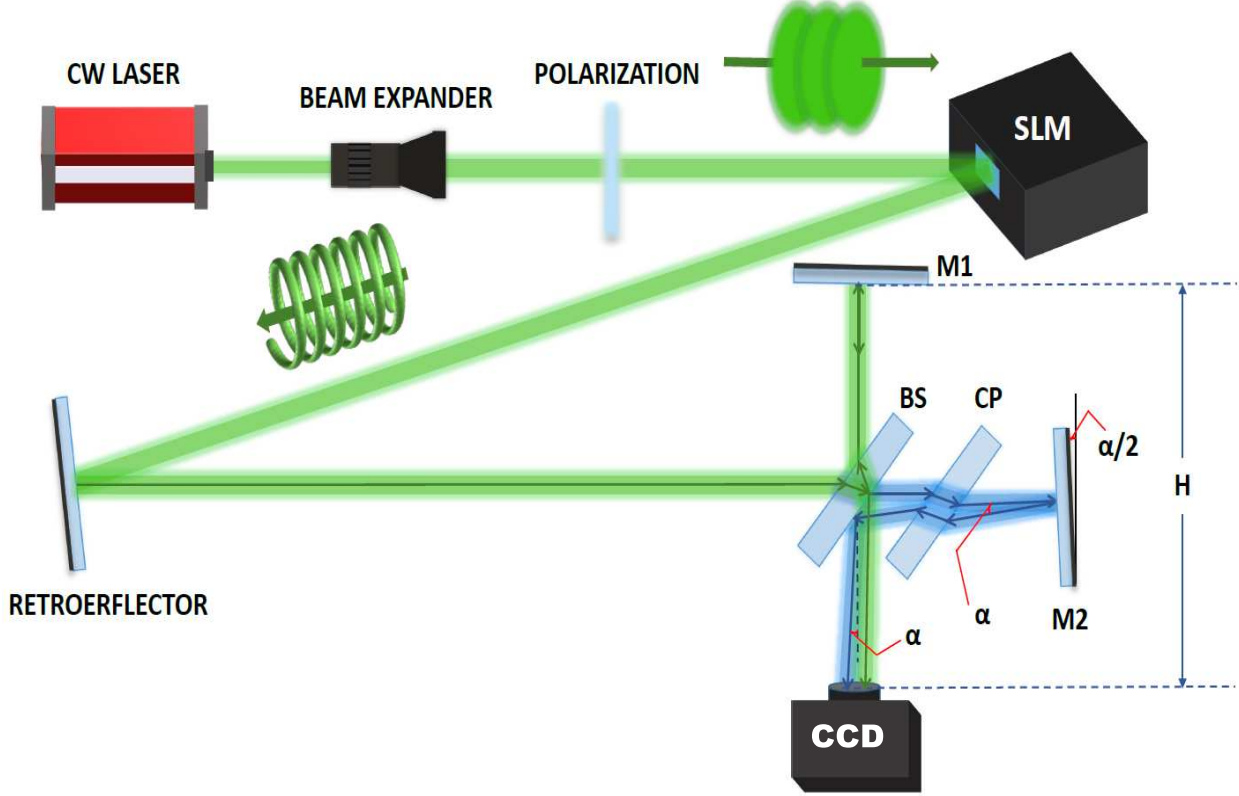


FIG. 1: Experimental setup. A CW 532 nm laser beam is modulated to be a Laguerre-Gauss beam by a SLM before being launched into the Michelson interferometer. Green and blue optical pathes are reflected by a fixed mirror $M1$ and a moving mirror $M2$. The interference pattern is imaged onto a cold CCD camera after the green light goes through the beam splitter (BS) and the blue light goes through the compensation plate (CP) and the BS. The inclined angle of the optical path is controlled by the moving mirror $M2$ by adjusting two screws in the device.

but can present unambiguously the inclined angle here. When the two vortex beams are received by the charge-coupled device (CCD), the interference pattern would be presented according to the following way given by the distribution of the total light intensity,

$$I = |E_{OAM1} + E_{OAM2}|^2 = A_1^2 + A_2^2 + 2A_1A_2\cos[(m_2\theta' - m_1\theta) + krs\sin\alpha], \quad (3)$$

where $(m_2\theta' - m_1\theta)$ is the phase difference caused by the coherent two vortex beams, which can be read from the interference pattern by the number and the direction of the branches. As the vortex beam is considered as self-coherent in our paper, the TCs and amplitudes for two vortex beams should be the same, i.e. $m_1 = m_2 = m$ and $A_1 = A_2 = A$. Thus, the

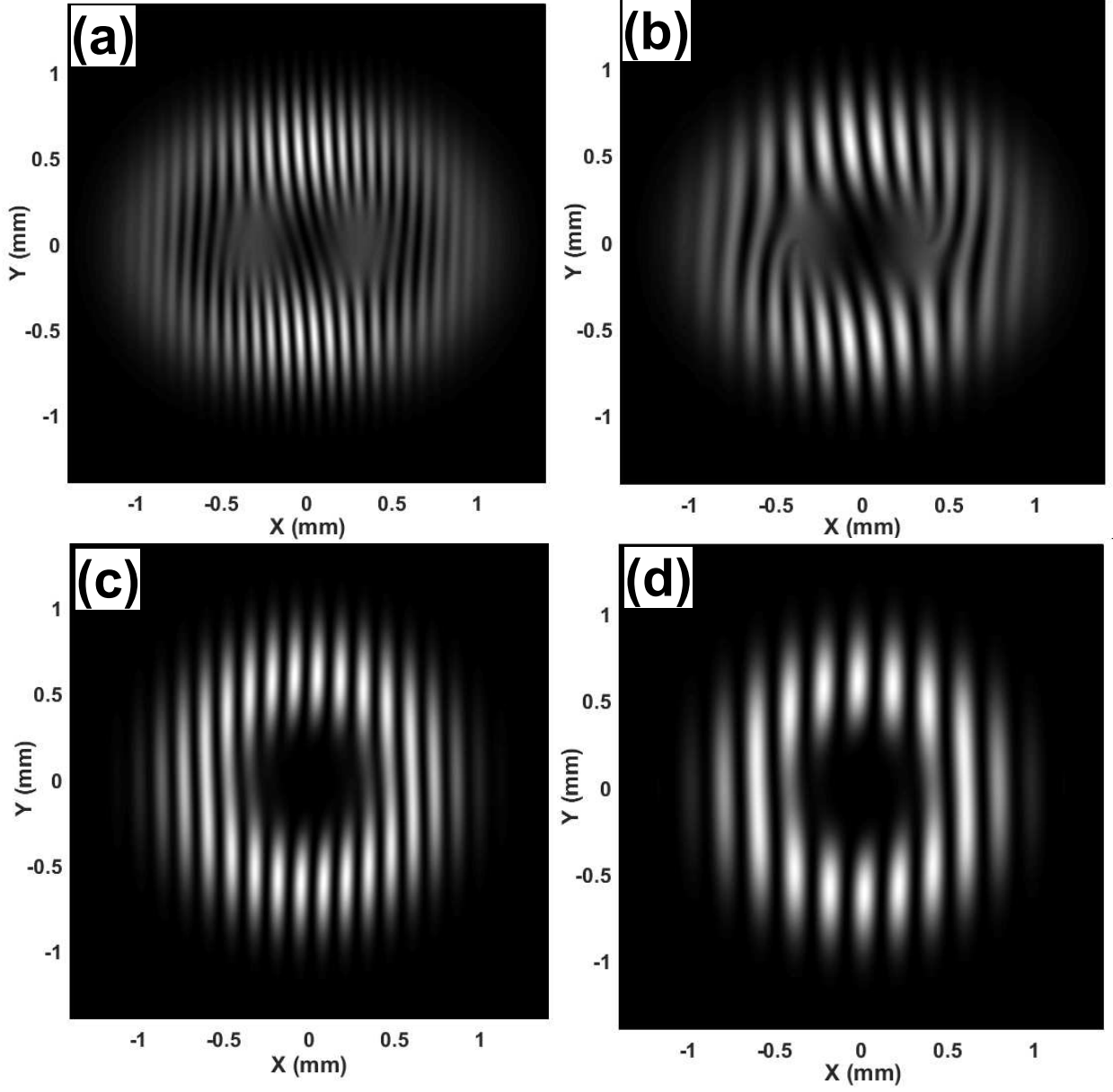


FIG. 2: Simulated results for the interference patterns with the different distance between the centers of two vortex beam: (a) $d = 0.60\text{mm}$; (b) $d = 0.36\text{mm}$; (c) $d = 0.24\text{mm}$; (d) $d = 0.12\text{mm}$. The value of TC for the vortices is taken as $m = 3$ for the simulation.

intensity distribution becomes

$$I = |E_{OAM1} + E_{OAM2}|^2 = 2A^2 + 2A^2 \cos[m(\theta' - \theta) + krsin\alpha], \quad (4)$$

At first, we simulate the interference using two LG vortex beams. It is noted that the width of the interference stripes will increase when the distance d (that is controlled by the inclined angle α in our paper) between the centers of the two vortex beams decreases, as

presented in Fig. 2. The branching number at each fork point denotes the number m of TC, and thus, the TC of the vortex beam can be detected by observing the number of the branches. Thus, the TC cannot be read from the Fig. 2 (d) in which the stripes is so fat that the number of branches is covered at the fork points. This is a new phenomena which is not observed before. In particular, it gives a limit for the measurement of the TC, and the related interpretation will be given below.

The existence of the measurement limit stems from two reason. One is fundamental which is limited by the distance d between the centers of two optical vortices or the inclined angle α . Another one is experimental which is limited by the pixel of the detector. In order to explain this clearly, we have to state the experimental setup to make the parameters be understood unambiguously.

In our experimental setup, a Michelson interferometer is used for the realization of the self-reference interferometry, and the adjustment of the mirrors can lead to the parallel and non-parallel optical paths. The practical instruments and optical paths are shown in Fig. 1. The continuous-wave (CW) of a Gauss laser beam is emitted from the semiconductor laser (CNI, China) with the mode TEM_{00} and the wavelength $532nm$. The diameter of the beam is expanded to $2mm$ by a beam expander. Then, it is modulated to be a typical vortex beam, a Laguerre-Gauss beam with the radial mode number $p = 0$ and TC $m = 3$ by a spatial light modulator (SLM, UPLabs, China). The conversion efficiency (or the zero-order diffraction efficiency) of the SLM for modulating the TEM_{00} beam to LG_{03} beam is about 80%. The generated vortex beam is pumped to the Michelson interferometer and is split into two coherent vortex beams which self-interfere on the imaging plane of a CCD. The interference pattern is produced in the cold CCD (Tucsen, China) with an array of 1912×1452 pixels (the size of each one is about $4.5 \mu m$). In Michelson interferometer, one of the optical path is reflected by a fixed mirror $M1$, and another optical path is reflected by a moving mirror $M2$. We can easily adjust two screws of $M2$ to change the inclined angle of the second optical path while the first path is fixed as the optical axis. The inclined angle α and the distance H between the imaging plane of the CCD camera and the mirror $M1$ (note that two armlengths are equal in our experiment) are marked in Fig. 1.

We firstly interpret the limit caused by the distance between the centers of two vortex beams or by the inclined angle. When the self-interference happens, the branching could appear in the interference pattern. In order to count the TC by the number of the branches

at the fork points, there are $(m + 2)$ discernable fringes at least in the region between the centers of two vortex beams, which is guaranteed by the relation,

$$d \geqslant (m + 2) \Delta d. \quad (5)$$

where $\Delta d = \lambda / \sin(\alpha)$ is the distance between two nearby bright fringes and the width for the bright and dark fringes is equal. Given the distance H , the distance d can be gotten using the inclined angle α as $d = H \tan(\alpha)$. Substitute this expression into the relation (5) and obtain the constraint for the detectable TC as,

$$m \leqslant \frac{H}{\lambda} \tan(\alpha) \sin(\alpha) - 2. \quad (6)$$

This shows that the larger the value of the inclined angle is, the larger the number of TC allowed to be measured is. At the same time, the distance d must be constrained to ensure that the singular points for the phase cannot exceed the edge of the intensity-overlapped region of two vortex beams, which requires

$$d = H \tan(\alpha) \leqslant r_0, \quad (7)$$

where r_0 is the radius of each beam. Compare the two relations (6) and (7), and we obtain a new relation to constrain the value of detectable TC,

$$m \leqslant \frac{r_0 \sin(\arctan(r_0/H))}{\lambda} - 2. \quad (8)$$

This is our central result. It shows that the maximal detectable TC ($m_{\max} = \frac{r_0 \sin(\arctan(r_0/H))}{\lambda} - 2$) is modulated by the radius of the beam and the distance H . Note that m_{\max} has the same changing trend with the radius of the beam as seen from the left plot of Fig. 3, but has the inverse changing trend with the distance H as seen from the right plot of Fig. 3. In our experiment, $\lambda = 532nm$, $H = 30cm$, and $r_0 = 1mm$, the constraint (8) gives $m \leqslant 4$, consistent with our experimental presentation. Larger values for TC can also be detected if the radius r_0 is increased or the distance H is decreased. If the radius r_0 increases to $1cm$ and the distance H decreases to $10cm$, the detectable TC can approach to 1880, which is possible but depends on the experimental conditions such as the pixel of the CCD camera and so on.

Then, we discuss the limit from the experimental conditions and focused on the influence from the pixel of the CCD camera. As discussed above, the distance Δd between two nearby

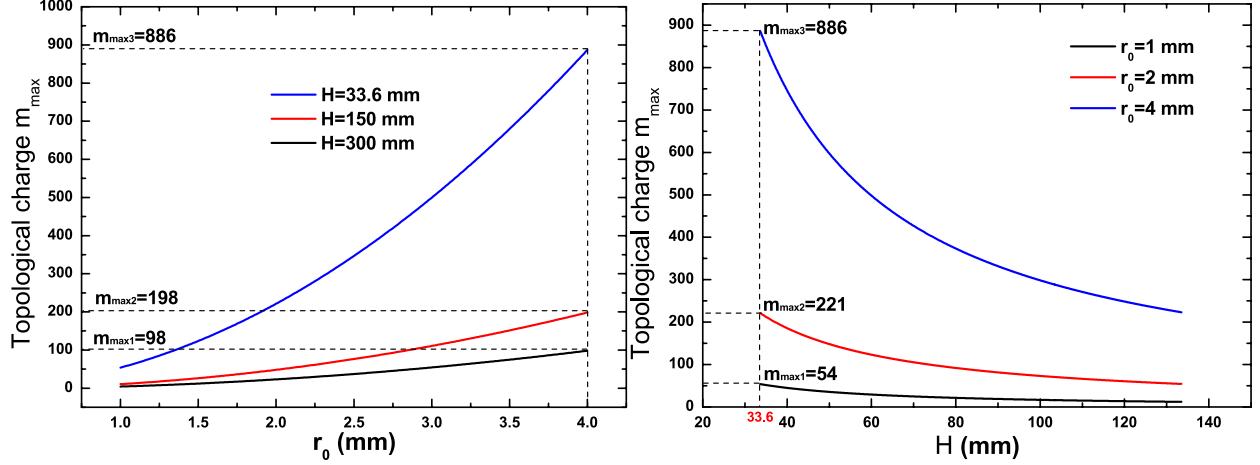


FIG. 3: Maximal detectable TC as a function of parameters r_0 and H . The left plot describes the change of maximal TC with r_0 for three different fixed H , and for every H , the value of maximal TC is marked for the experimentally allowed largest value of r_0 . The right plot describes the change of maximal TC with H for three different fixed r_0 , and for every r_0 , the value of maximal TC is marked for the experimentally smallest value of H .

bright fringes is $\Delta d = \lambda / \sin(\alpha)$. Thus, the spatial frequency of the fringes for one pixel d_{pixel} can be expressed as $f = d_{\text{pixel}} / \Delta d = d_{\text{pixel}} \sin(\alpha) / \lambda$, which means that when the observation is made at the imaging plane of CCD camera, the number of fringes observed at each pixel is f . In order to distinguish the fringes clearly, the number of the fringes appeared on CCD should be equal to that obtained through the interference, which means that a single fringe should be converted on a single pixel of CCD. Mathematically, it requires $f \leq 1$ or

$$\alpha \leq \arcsin\left(\frac{\lambda}{d_{\text{pixel}}}\right). \quad (9)$$

This shows the geometric parameter α is constrained by the experimental condition and cannot be increased or decreased at random. In our experiment, $\lambda = 532\text{nm}$, $d_{\text{pixel}} = 4.5\mu\text{m}$ which gives that the inclined angle cannot be more than $\alpha_{\max} \simeq 0.118$.

According to our CCD, the radius of the beam can only increase to $r_0 = 4\text{mm}$ at most which demands

$$H \geq \frac{r_0}{\tan(\alpha_{\max})} \simeq 33.6\text{mm}, \quad (10)$$

where the relations (7) and (9) are used. Together with the relation (8), it shows that the distance H cannot be decreased at random and the radius r_0 cannot be increased at random for the purpose of detecting large TC, and they must satisfy such relation as (10)

that present the experimental constraint. The maximal TC that can be detected is 886 by substituting $H = 33.6mm$ and $r_0 = 4mm$ into the relation (8), but in the practical experimental implementation, the distance H cannot take so small value.

We also present experimentally the limit of measuring TC by self-reference interferometry using the setup in Fig. 1. The experiment begins from so far distance between two vortex beams that the two beams are not overlapped, as given in Fig. 4(a), to the distance where no branching can be observed, as given in Fig. 4(h). It is seen that the stripes become fatter as the two vortex beams approach to each other, which means that the experimental measurement of TC will be limited when the stripes becomes so fat that the two fork points cannot be distinguished, as shown in Fig. 4 (g) and (h). In particular, the interference at the least distance d (about $0.6mm$) where the branching just cannot be observed is presented in Fig. 4 (g).

III. MEASUREMENT OF TOPOLOGICAL CHARGES

As discussed above, the self-reference interferometry has a constraint for the detection of TC. Only if the detection is allowed and does not exceed the range of the constraint, this method is still nice. In this section, we will present the detection of TC for several different cases.

In Fig. 5, we present three different cases for the propagation of the two vortex beams. For the Fig. 5 (a), the two beams propagates along the parallel paths, but the optical centers are overlapped partly. For the Fig. 5 (b) and (c), the two beams propagates non-parallelly, in which the blue path is inclined from the green one at the angle α . In particular, the optical centers are overlapped completely at the received place in Fig. 5 (b). All the three cases have the overlapped parts for the two vortex beams to ensure the interference can occur.

When two optical paths are parallel ($\alpha = 0$) but the optical centers of the two vortex beams are misaligned ($\theta' \neq \theta$), the interference pattern appears according to the distribution of the light intensity

$$I = |E_{OAM1} + E_{OAM2}|^2 = 2A^2 + 2A^2 \cos[m(\theta' - \theta)], \quad (11)$$

which derives from Eq. (4) with the zero inclined angle. The interference pattern looks

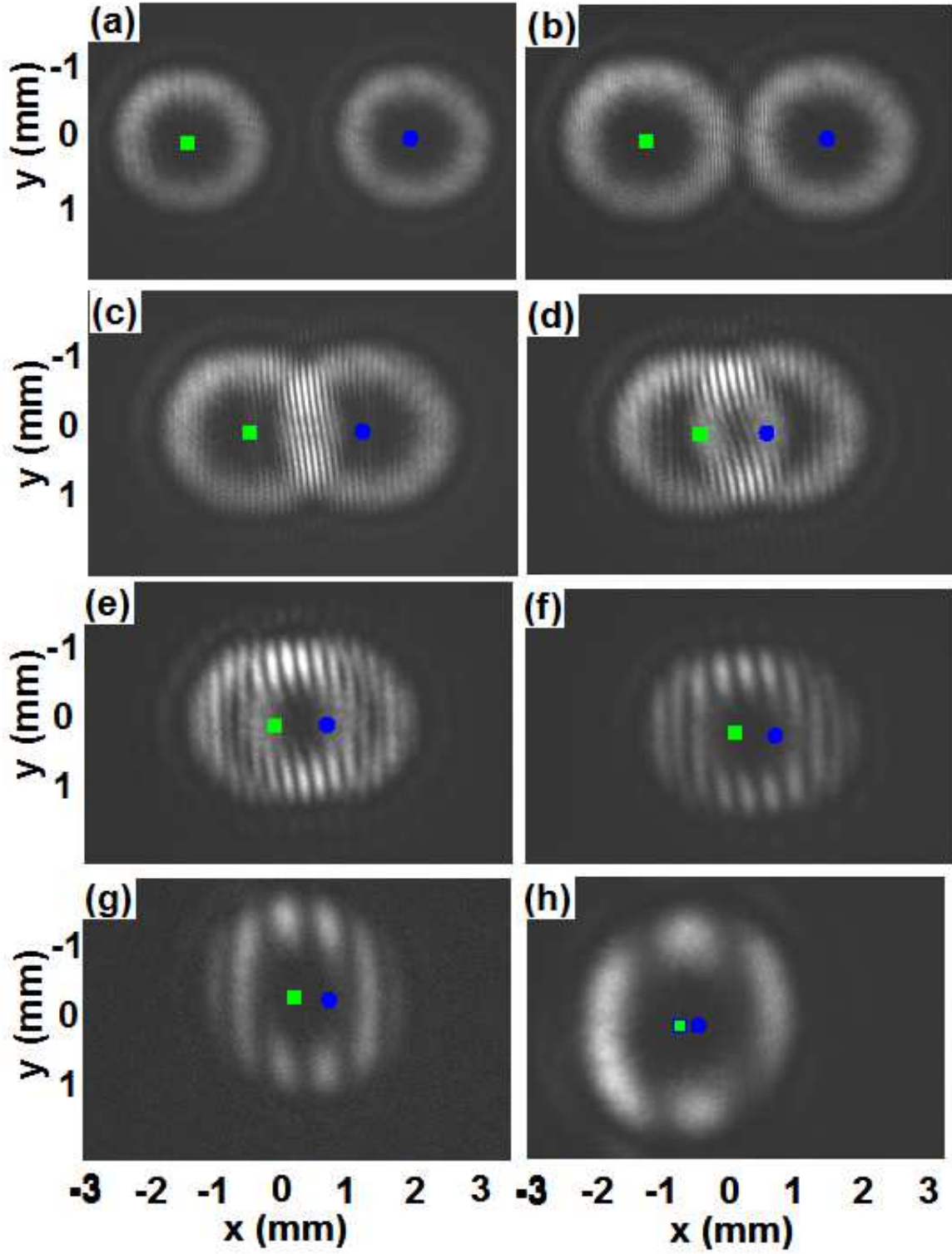


FIG. 4: Experimental results for the interference patterns of two vortex beams using self-reference method when the distance between centers of two vortex beams decreases gradually and uniformly from 3.2mm to 0.3mm , with $m = 3$ for the value of TC of the vortices .

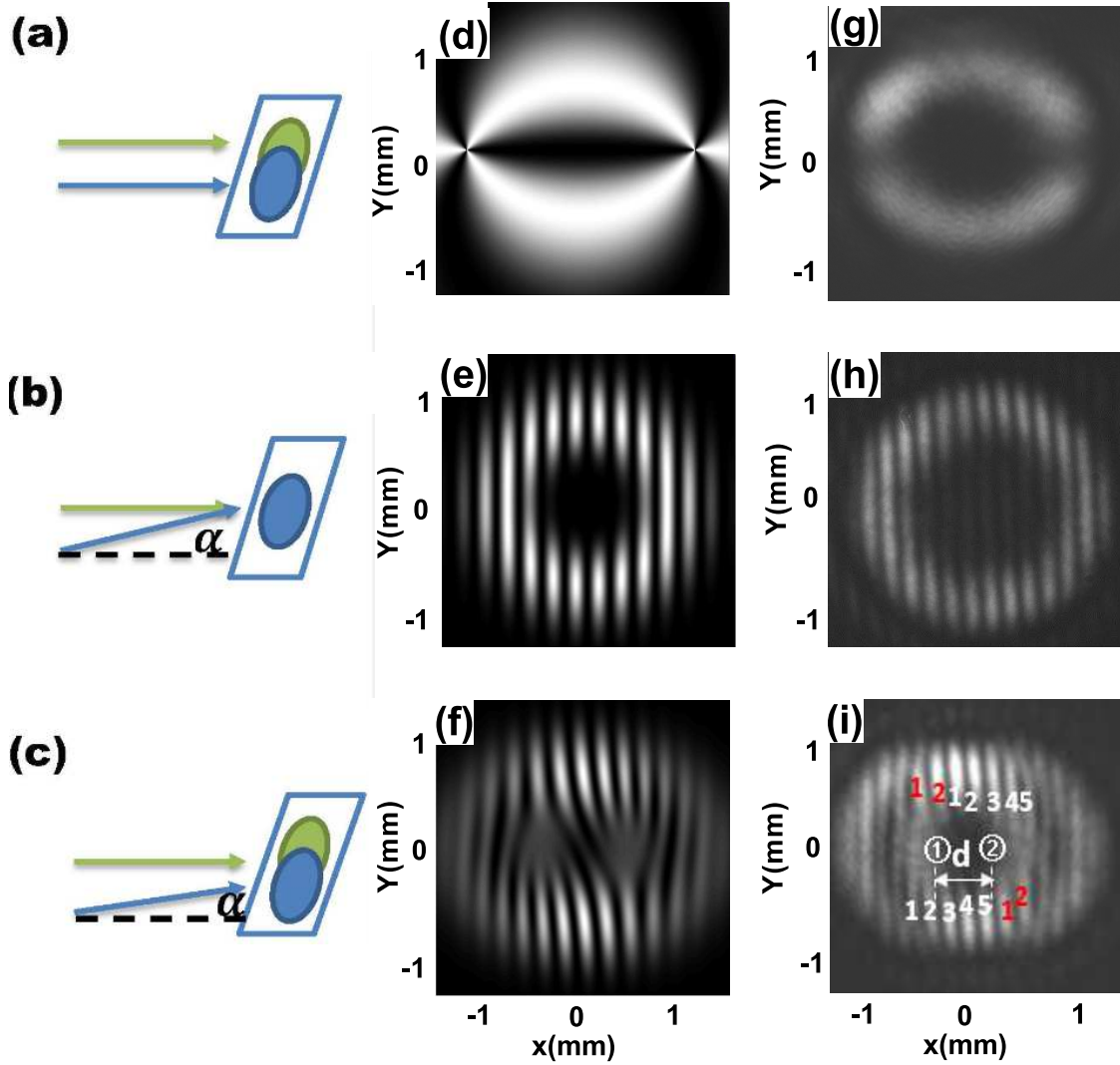


FIG. 5: Schematic diagram of optical paths, simulated and experimental results for different cases. (a)-(c) are the different cases for the two optical pathes, their corresponding interference patterns are presented in (d)-(f) using numerical method, and their corresponding experimental results are given in (g)-(i). The blue and green arrow lines represent two vortex beams. α is the inclined angle of one of the vortex beams. The value of TC for the vortices is $m = 3$ in these figures.

like two arcs connecting two singularities shown in Fig. 5 (d) numerically and Fig. 5(g) experimentally.

For the case presented in Fig. 5 (b) ($\alpha \neq 0, \theta' = \theta$), two phase singularities coincide, and the interference pattern is given by the straight stripes without a fork point, as shown in

Fig. 5 (e) numerically and Fig. 5(h) experimentally.

Considering misaligned centers with shearing interference ($\alpha \neq 0, \theta' \neq \theta$) in Fig. 5 (c), there are two phase singularities seen from the fork points introduced by θ' and θ , respectively. The interference pattern could be interpreted with the pattern of two opposite-directional forks as shown in Fig. 5 (f) numerically and Fig. 5 (i) experimentally, like a “classical” interference between a vortex beam and a plane beam. Meanwhile, the TC of the vortex beam can be detected by observing the branching number.

Besides the three cases, there is a trivial one that two optical paths are completely overlapped ($\alpha = 0, \theta' = \theta$) which is not plotted, since there is no pattern appearing due to the interference cancellation.

Note that we use the inclined angle to modulate the distance between the centers of two vortex beams. Thus, we can check if the two mirrors $M1$ and $M2$ in the Michelson interferometer are vertical based on the self-reference interferometry. The inclination of one of the paths brings about the transverse wave vector component to interfere with the angular wave vector component, which leads to the change of the interference pattern. When the inclination exists and the two paths are not parallel, the TC can be observed evidently. When the ray of light reflected by $M1$ and the ray of light reflected by $M2$ are strictly vertical, two vortex beams interfere without branches. So, the appearance of the branches in the interference pattern is an indication that the two mirrors $M1$ and $M2$ are not vertical, which provides a precise measurement for a slight inclination of the mirror $M2$. Moreover, different methods using the stripes of an interference pattern to infer that the mirror $M2$ is tilted is also very well established, the interested readers can refer to [38].

IV. CONCLUSIONS

In this paper, we investigate the self-reference interferometry based on the Michelson interferometer, which can be used for the measurement of TC of the optical vortex or checking whether the propagating paths of two vortex beams are parallel. In this method, the coherent beams are derived from the same vortex beam modified by the SLM and the inclination is controlled by adjusting the mirror $M2$ of the interferometer. Novelly, we find that the detection of TC must satisfy some constrained conditions. We study the conditions in detail and obtain that the limits of measurement (the maximal values of detectable

TC) are different for the different values taken for the physical parameters as the radius of the beam or the distance H . Thus, TC of the optical vortex cannot be detected from the self-reference interferometry beyond these constrained conditions. These were not realized before. As a practical application, we analyze several cases theoretically and experimentally for demonstrating the relation among the interference pattern, the inclination and the parallelism of the optical paths within the allowed range of the constrained conditions. This is also significant in the practical operation using the Michelson interferometer.

V. ACKNOWLEDGMENTS

We would like to the anonymous referees for their critical and helpful suggestions and comments. This work is supported by the NSFC under Grant No. 11654001.

VI. REFERENCES

-
- [1] P. Couillet, L. Gil, and F. Rocca, Optical vortices. *Opt. Commun.* 73, 403 (1989).
 - [2] Y. Shen, X. Wang, Z. Xie, C. Min, X. Fu, Q. Liu, M. Gong, and X. Yuan, Optical vortices 30 years on: OAM manipulation from topological charge to multiple singularities. *Light: Science and Application* 8, 90 (2019).
 - [3] A. Grover, Jr. Swartzlander, Peering in to darkness with a vortex spatial filter. *Opt. Lett.* 26, 497 (2001).
 - [4] D. Palacios, D. Rozas, and G. A. Swartzlander, Observed scattering into a dark optical vortex core. *Phys. Rev. Lett.* 88, 103902 (2002).
 - [5] L. Allen, M. W. Beijersbergen, R. J. C. Spreeuw, and J. P. Woerdman, Orbital Angular-Momentum of Light and the Transformation of Laguerre-Gaussian Laser Modes. *Phys. Rev. A* 45, 8185 (1992).
 - [6] M. W. Beijersbergen, L. Allen, H. E. L. O. van der Veen, and J. P. Woerdman, Astigmatic laser mode converters and transfer of orbital angular momentum. *Opt. Commun.* 96, 123 (1993).

- [7] M. W. Beijersbergen, R. P. C. Coerwinkel, M. Kristensen, and J. P. Woerdman, Helical wave front laser beams produced with a spiral phase plate. *Opt. Comm.* 112, 321 (1994).
- [8] N. R. Heckenberg, R. McDuff, C. P. Smith, and A. G. White, Generation of optical phase singularities by computer-generated holograms. *Opt. Lett.* 17, 221 (1992).
- [9] J. E. Curtis, B. A. Koss, D. G. Grier, Dynamic holographic optical tweezers. *Opt. Comm.* 207, (2002).
- [10] J. Zeng, L. Li, X. Yang, and J. Gao, Generating and separating twisted light by gradient-rotation split-ring antenna metasurfaces. *Nano Letters.* 16, 3101 (2016).
- [11] D. Veksler, E. Maguid, N. Shitrit, D. Ozeri, V. Kleiner, and E. Hasman, Multiple wavefront shaping by metasurface based on mixed random antenna groups. *ACS Photonics* 2, 661 (2015).
- [12] K. T. Gahagan and G. A. Swartzlander, Optical vortex trapping of particles. *Opt. Lett.* 21, 827 (1996).
- [13] L. Li, C. Chang, X. Yuan, C. Yuan, S. Feng, S. Nie, and J. Ding, Generation of optical vortex array along arbitrary curvilinear arrangement. *Opt. Express* 26, 9798 (2018).
- [14] A. Mair, A. Vaziri, G. Weihs, and A. Zeilinger, Entanglement of the orbital angular momentum states of photons. *Nature* 412, 313 (2001).
- [15] B. Ndagano, I. Nape, M. A. Cox, C. Rosales-Guzman, and A. Forbes, Creation and detection of vector vortex modes for classical and quantum communication. *J. Lightwave Technol.* 36, 292 (2018).
- [16] B. Spektor, A. Normatov, J. Shamir, Singular beam microscopy. *Appl. Opt.* 47, A78 (2008).
- [17] A. Serrano-Trujillo and M. E. Anderson, Surface profilometry using vortex beams generated with a spatial light modulator. *Opt. Commun.* 427, 557 (2018).
- [18] W. Cheng, X. Liu, and P. Polynkin, Simultaneously spatially and temporally focused femtosecond vortex beams for laser micromachining. *J. Opt. Soc. Am. B* 35, B16 (2018).
- [19] C. Hnatovsky, V. G. Shvedov, W. Krolikowski, and A. V. Rode, Materials processing with a tightly focused femtosecond laser vortex pulse. *Opt. Lett.* 35, 3417 (2010).
- [20] M. P. J. Lavery, Detection of a spinning object using light's orbital angular momentum. *Science* 341, 1175 (2013).
- [21] B. Liu, H. Giddens, Y. Li, Y. He, and W.-S. Wai, Design and experimental demonstration of Doppler cloak from spatiotemporally modulated metamaterials based on rotational Doppler effect. *Opt. Express* 28, 3745 (2020).

- [22] F. Marino, Acoustic black holes in a two-dimensional “photon fluid”. *Phys. Rev. A* 78, 063804 (2008).
- [23] D. Vocke, C. Maitland, and A. Prain, Rotating black hole geometries in a two-dimensional photon superfluid. *Optica* 5, 2334 (2018).
- [24] D. Fu, D. Chen, R. Liu, Y. Wang, H. Gao, F. Li and P. Zhang, Probing the topological charge of a vortex beam with dynamic angular double slits. *Opt. Lett.* 40, 788 (2015).
- [25] S. Zheng and J. Wang, Measuring orbital angular momentum (OAM) states of vortex beams with annular gratings. *Sci. Rep.* 7, 40781 (2017).
- [26] M. V. Vasnetsov, J. P. Torres, D. V. Petrov, and L. Torner, Observation of the orbital angular momentum spectrum of a light beam. *Opt. Lett.* 28, 2285 (2003).
- [27] N. Yu and F. Capasso, Flat optics with designer metasurfaces. *Nat. Mater.* 13, 139 (2014).
- [28] J. Jin, J. Luo, X. Zhang, H. Gao, X. Li, M. Pu, P. Gao, Z. Zhao, and X. Luo, Generation and detection of orbital angular momentum via metasurface. *Sci. Rep.* 6, 24286 (2016).
- [29] H. I. Sztul and R. R. Alfano, Double-slit interference with Laguerre–Gaussian beams. *Opt. Lett.* 31, 999 (2006).
- [30] B. Khajavi and E. J. Galvez, Determining topological charge of an optical beam using a wedged optical flat. *Opt. Lett.* 42, 1516 (2017).
- [31] G. G. Liu, K. Wang, Y.-H. Lee, D. Wang, P. P. Li, F. Gou, Y. Li, C. Tu, S. T. Wu, and H. T. Wang, Measurement of the topological charge and index of vortex vector optical fields with a space-variant half-wave plate. *Opt. Lett.* 43, 823 (2018).
- [32] H.-C. Huang, Y.-T. Lin, and M.-F. Shih, Measuring the fractional orbital angular momentum of a vortex light beam by cascaded Mach–Zehnder interferometers. *Opt. Comm.* 285, 383 (2012).
- [33] P. Kumar and N. K. Nishchal, Modified Mach–Zehnder interferometer for determining the high-order topological charge of Laguerre–Gaussian vortex beams. *J. Opt. Soc. Am. A* 36, 1447 (2019).
- [34] K. N. Gavril’eva, A. Mermoul, A. A. Sevryugin, E. V. Shubenkova, M. Touil, I. M. Tursunov, E. A. Efremova, and V. Yu. Venediktov, Detection of optical vortices using cyclic, rotational and reversal shearing interferometers. *Optics and Laser Technology* 113, 374 (2019).
- [35] X. Guo, Z. Meng, J. Li, J.-Z. Yang, M. Aili, and A.-N. Zhang, The interference properties of single-photon vortex beams in Mach–Zehnder interferometer. *Appl. Phys. Lett.* 119, 011103

- (2021).
- [36] P. Kurzynowski, M. Borwińska, and J. Masajada, Optical vortex sign determination using self-interference methods. *Optica Applicata* XL(1), 165 (2010).
- [37] B. Lan, C. Liu, D. Rui, M. Chen, F. Shen, and H. Xian, The topological charge measurement of vortex beam based on dislocation self-reference interferometry. *Physica Scripta* 94, 055502 (2019).
- [38] P. Hariharan, *Basics of Interferometry* (Second Edition). Elsevier Academic Press, Holland (2007).